Å²/molecule for R(0); π = 38 mN/m and 87 Å²/molecule for R(1); and π = 38 mN/m and 108 Å²/molecule for R(2). Previous work on LB films of similar molecules has been reported [D. B. Amabilino et al., New J. Chem. **1998**, 959 (1998)].

12. V. Balzani, M. Gomez-Lopez, J. F. Stoddart, Acc. Chem. Res. **31**, 405 (1998).
13. A. Credi, V. Balzani, S. J. Langford, J. F. Stoddart, J. Am. Chem. Soc. **119**, 2679 (1997).
14. C. Zhou, M. R. Deshpande, M. A. Reed, L. Jones II, J. M. Tour, Appl. Phys. Lett. **71**, 611 (1997).
15. These devices were operated under ambient conditions and no effort was made to exclude water or oxygen vapor. Their performance degraded over a period of a few days, similar to what would be expected for an unpackaged polymer-based electron-

ic device. At voltages near ±3 V, the junction breaks down and an open circuit is measured. The overall device yield, based on measuring several hundred devices over ~20 separate fabrication runs, was greater than 95%.
16. We monitored the oxidation of the devices by holding the device at a positive (oxidizing) bias for extended periods, and then monitoring the current through the device at −2.0 V. Oxidation at +0.7 V took several minutes, but oxidation only took a few seconds at voltages above +1 V. When devices were oxidized at +0.5 V, the current flow at −2.0 V dropped only very slightly—by about 1% per minute of oxidation.
17. R. M. Feenstra, J. A. Stroscio, A. P. Fein, Surf. Sci. **181**, 295 (1987).

18. W. B. Davis, W. A. Svec, M. A. Ratner, M. R. Wasielewski, Nature **396**, 60 (1998).
19. K. W. Hipps and U. Mazur, J. Phys. Chem. **98**, 5824 (1994).
20. E. E. Polymeropoulos and J. Sagiv, J. Chem. Phys. **69**, 1836 (1978).
21. By the term "crosstalk," we are referring to complications that might arise when separate devices share a common electrode. One complication might be the unintentional oxidation of a device.
22. This work was supported by the Office of Naval Research (contract N00014-98-1-0422), the NSF-GOALI program, and Defense Advance Research Projects Agency.

Electrostatic Repulsion of Positively Charged Vesicles and Negatively Charged Objects

Helim Aranda-Espinoza,[1]* Yi Chen,[2] Nily Dan,[1]* T. C. Lubensky,[2] Philip Nelson,[2]† Laurence Ramos,[3] D. A. Weitz[2]‡

A positively charged, mixed bilayer vesicle in the presence of negatively charged surfaces (for example, colloidal particles) can spontaneously partition into an adhesion zone of definite area and another zone that repels additional negative objects. Although the membrane itself has nonnegative charge in the repulsive zone, negative counterions on the interior of the vesicle spontaneously aggregate there and present a net negative charge to the exterior. Beyond the fundamental result that oppositely charged objects can repel, this mechanism helps to explain recent experiments on surfactant vesicles.

Opposite charges attract in vacuum. Two ionizable objects in an electrolyte such as water form a more complex system, but nevertheless, in many situations a simple rule of thumb applies: As two planar surfaces approach from infinity, they initially attract if oppositely charged, with a screened Coulomb potential (1).

The analysis here was motivated by two sets of experimental observations that defy the familiar rule above (2, 3). Bilayer vesicles were prepared from a mixture of cationic (positively charged) and neutral surfactants. In one case, vesicles were allowed to adhere to a negatively charged substrate (2), while in the other, negatively charged colloidal particles were introduced into suspensions of vesicles and the resulting self-assembled struc-

tures monitored (3). The puzzling observation was that despite the high charge on the vesicles, they were not uniformly attractive to the particles or surfaces, but instead separated macroscopically into adhesive and nonadhesive zones (Fig. 1). The vesicle diameter was typically 20 μm; the Debye screening length $1/\kappa$ was much smaller, between 1 and 10 nm (4). Because membranes in living cells also include bilayers made from mixtures of negatively charged and neutral lipids (5), phenomena like the ones reported here might occur generally.

The observed behavior is disturbingly counterintuitive and raises several questions: Why should adhesion to one zone of the membrane affect adhesion hundreds of screening lengths away? More urgently, why should electrostatic adhesion saturate in this way? How can oppositely charged objects repel?

The key to the puzzle is a subtle interplay between the entropic and electrostatic effects of the mobile counterions and laterally mobile lipids, which leads to a thermodynamic instability: The equilibrium state involves the coexistence of adhesive and repulsive zones in the membrane. The latter repel incoming negative objects by recruiting negative counterions on the interior face. The effects of demixing on membrane adhesion have been

studied by other groups [for example, (2, 6)]. Our mechanism differs from earlier ones by including cooperative effects between counterions on both sides of an impermeable membrane. This effect can lead to adhesion saturation, a full discussion of which will appear elsewhere (7).

At least three possible equilibrium states could result when a mixed bilayer vesicle encounters charged surfaces: (i) The vesicle composition could remain uniform, and thus be uniformly attractive to the approaching surfaces. In this case, the vesicle should end up completely covered by particles (or tense and tightly adhering to the substrate). (ii) Alternately, binding could cause total lateral demixing of the charged and neutral surfactants in the membrane, and lead to a charge-depleted zone with no attraction to negative objects. One can easily show, however, that totally eliminating charged surfactants from the latter zone comes at a high cost in lateral distribution entropy; instead, enough residual charge will always remain to make the depleted zone quite attractive. Thus, one would expect at most (iii) a coexistence between high charge density (tight adhesion) and low charge density (weak adhesion) zones.

In the experiments mentioned, however, often none of the above three expectations was realized. Instead, adhesion saturated at some optimal coverage. Once this point was reached, the colloidal particles in (3) were not seen to leave or join the vesicle. Indeed, particles in suspension are seen to approach the vesicle, then bounce off. Similarly, the experiment in (2) found "blistering" in the contact region instead of uniform tight contact.

To confront this paradox, we begin with Parsegian and Gingell's classic analysis of the attraction of oppositely charged, planar surfaces (8). The authors studied the interaction of two infinite parallel planes with fixed bound surface charge densities $\sigma_+ > 0$ and $\sigma_- < 0$. Between the planes, a gap of width ℓ contains water, a dielectric medium with dielectric constant (9) $\epsilon = 80\epsilon_0$ with mobile point charges (ions) supplied by an external reservoir. We will consider all ions to be univalent, as in the experiment of (3). The

[1]Department of Chemical Engineering, University of Delaware, Newark, DE 19716, USA. [2]Department of Physics and Astronomy, University of Pennsylvania, Philadelphia, PA 19104 USA. [3]Groupe de Dynamique des Phases Condensées, Case 26, Université de Montpellier II, Place E. Bataillon, 34095 Montpellier Cedex 05, France.

*Address after 1 September 1999: Department of Chemical Engineering, Drexel University, Philadelphia, PA 19104, USA.
†To whom correspondence should be addressed.
‡Address after 1 September 1999: Department of Physics, Harvard University, Cambridge, MA 02138, USA.

reservoir has fixed density $\hat{n}$ of positive ions and an equal number of negative ions. To either side of the gap lie infinite dielectrics with no free charges.

In this situation, Parsegian and Gingell found that oppositely charged surfaces initially attract as they are brought in from infinite separation. The physical mechanism for the attraction is revealing: As the two surfaces' counterion clouds begin to overlap, a positive counterion from the negative surface can join a negative counterion from the positive surface; the pair then escapes to the infinite reservoir, gaining entropy, without any net separation of charge. The process continues as the surfaces approach, until one counterion cloud is completely exhausted. If $|\sigma_-| > \sigma_+$, then at this point only positive counterions remain in the gap. These residual ions cannot escape, because that would leave a nonzero net charge in the gap (in the assumed infinite planar geometry, net charge carries an infinite cost in electric field energy).

At some separation ℓ_*, then, the osmotic pressure of the trapped residual counterions balances the electrostatic attraction of the plates. Nevertheless, the total free energy change for bringing the plates together is always negative: Oppositely charged surfaces always adhere (8). This adhesion energy per area is given by $W \equiv f(\ell_*) - f(\infty) = -(\sigma_+)^2/\epsilon\kappa$, where κ is the inverse screening length. Remarkably, W is completely independent of the majority charge density σ_- (2). In light of the above physical picture, we can readily interpret this fact: The total counterion release is limited by the smaller of the two counterion populations.

Thus, the physical situation studied by Parsegian and Gingell does not exhibit adhesion saturation. Fortunately, the general situation studied here differs in three key ways from theirs (see Fig. 2, A and B): (i) One of the surfaces is an infinite dielectric of fixed charge density σ_-, as above, but the other contains a fluid mixture of charged and neutral elements. Thus, the latter's charge density σ_+ may vary, with surface average fixed to some value $\sigma_{+,av}$. (ii) The positive surface is assumed to be a membrane bounding a closed vesicle of surface area A, not the boundary of a solid dielectric body. The membrane separates two regions with the same salt concentration $\hat{n}$ far from the membrane. (iii) We have coexistence of two zones on the membrane: an attachment zone "a" similar to the one studied by Parsegian and Gingell and a second zone "b," which will eventually prove to be unattached (we do not assume this).

Because the sizes of the colloidal spheres and the vesicle are much bigger than the screening length, our geometry is essentially planar (Fig. 2B). (This idealization is self-consistent, as the equilibrium spacing ℓ_* found below will prove to be of order the

screening length.) For the same reason, we can neglect fringe fields at the boundaries of the zones "a" and "b."

Before proceeding with any calculations, we now sketch the new physics which can arise in the general situation described by points (i) to (iii) above. For concreteness, suppose that half the vesicle's counterions, with charge $A\sigma_{+,av}/2$, are confined to the interior of the vesicle and half to the exterior.

One may be tempted to ignore the interior counterions altogether, in light of the fact that bilayer membranes are highly impermeable

to ions (10). Indeed, counterions trapped inside the vesicle cannot participate directly in the mechanism described above for electrostatic adhesion, since they cannot pair with exterior counterions and escape together to infinity. Accordingly, let us momentarily suppose that the density of interior counterions is fixed.

In this situation (fixed interior counterions), Nardi et al. noted that zone "a" can recruit additional charged surfactants from zone "b" in order to liberate their counterions and improve the adhesion (Fig. 2, B and C)
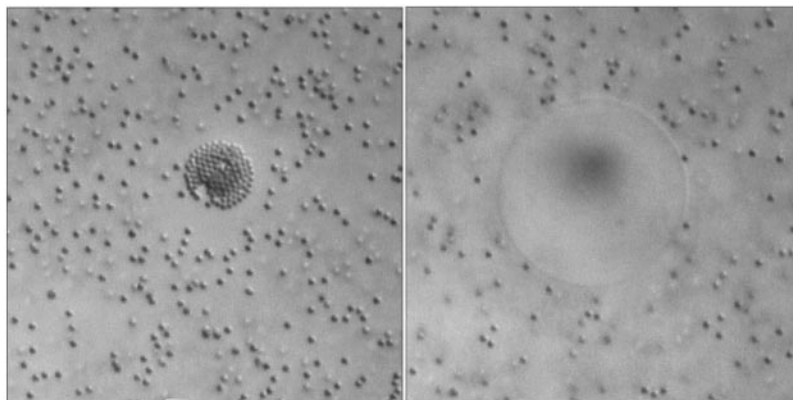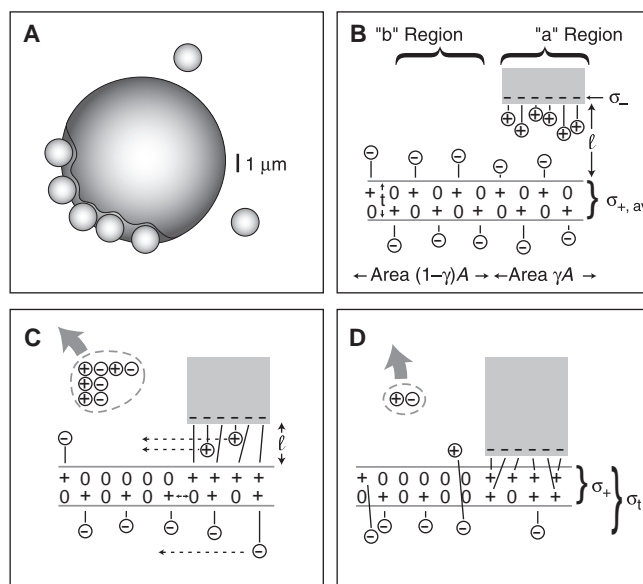

Fig. 1. A self-limited array of latex spheres on a charged surfactant vesicle at room temperature (3). The spheres are on the surface of a vesicle viewed in differential interference microscopy, focusing on the array itself (left) or on the vesicle equator (right). The membrane is a mixture of cationic and neutral surfactants (DDAB and Triton X, respectively, with octanol added to stabilize bilayer structures). The sphere diameter is 1 μm; the sphere volume fraction is 0.004.

Fig. 2. (**A**) Schematic of the geometry. A vesicle of mixed neutral and cationic surfactants binds a few anionic objects, then stops, even though further spheres are available. (**B**) Planar idealization when an approaching charged dielectric (shaded, top right) is still far away from the membrane. The membrane interior is at the bottom of the figure. The zeros denote neutral surfactants, "+" signs the charged surfactants. Circled "+" and "−" signs denote counterions in solution. The solid vertical lines joining charges are fictitious elastic tethers representing intuitively the electric field lines; the requirement of charge neutrality translates visually into the requirement that all charges be tied in this way. (**C**) Redistribution of charges when the negative dielectric approaches the membrane, if we forbid any charge separation across the membrane. Four pairs of counterions have been released to infinity (top left). The interior monolayer, and its counterion cloud, are unchanged from (B). Zone "b" presents a net of one positive charge to the vesicle exterior and so attracts further incoming negative objects. Dashed horizontal arrows indicate a further rearrangement of charges allowed once we relax the constraint of zero charge separation across the membrane. (**D**) The resulting state after the migrations indicated by dashed arrows in (C). One additional counterion pair has been released to infinity and the adhesion gap has narrowed. The net charge of the bilayer plus interior counterions in zone "b" has reversed sign relative to (C).

(2). The entropic tendency of the charged and uncharged surfactants to remain mixed opposes this redistribution, however, and the resulting adhesion is a compromise between the two effects. Zone "b" will still have non-negative charge and will still remain quite attractive to further colloidal particles; there is no adhesion saturation.

The argument just given, however, neglects the ability of interior counterions to move laterally. As shown in Fig. 2C, the approaching exterior negative object will push negative interior counterions out of zone "a" and into zone "b," where they can overwhelm the residual positive membrane charge and effectively reverse its sign.

This rearrangement liberates exterior counterions from both zones (Fig. 2D), enhancing the adhesion. The capacitive energy cost of separating charge across a membrane in this way is significant, because of the low dielectric constant $\epsilon_m \approx 2\epsilon_0$ of the hydrocarbon tails of lipids and other surfactants. Nevertheless, the cost is initially zero, being proportional to the square of the charge separated; hence, there will always be some lateral rearrangement inside the vesicle, as indicated by the dashed arrows in Fig. 2C; Fig. 2D is the result. If this rearrangement reverses the effective membrane charge, it will lead to active repulsion in the nonadhesion "b" zone.

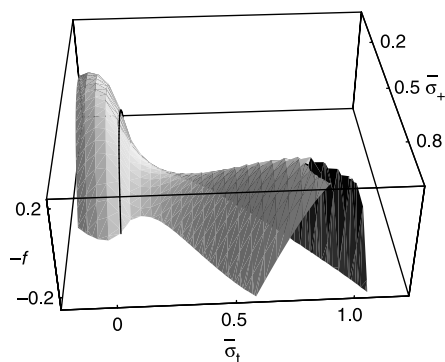We will now show that the scenario just

Fig. 3. Free energy density for a fictitious, infinitely thin membrane. The variables $\bar{\sigma}_t$ and $\bar{\sigma}_+$ are nondimensional forms of the charge densities σ_+ and σ_t in Fig. 2D. For easier visualization, we have inverted the figure, rescaled, and added a linear function, plotting $-\kappa f(\bar{\sigma}_+, \bar{\sigma}_t)/1000\hat{n}k_BT +$ 218.0 + 6.0$\bar{\sigma}_+$ − 11.4$\bar{\sigma}_t$ instead of f. For illustration we have taken the average membrane composition $\bar{\sigma}_{+,\mathrm{av}} = 0.5$ (corresponding to 1:1 mole fraction of charged surfactant), the normalized colloidal particle charge $|\bar{\sigma}_-| = 1.5$, and $\beta = 0.006$ (see text). The solid curve is the locus of points where $\bar{\sigma}_- = 0$; points to the left of this curve represent charge-reversed states. The geometric fact that the surface shown has two hills on opposite sides of the solid curve implies that the system's ground state consists of two coexisting zones, one of which is charge-reversed. The common-tangent construction from thermodynamics determines the composition of the two zones.

sketched can actually occur under a broad range of experimentally realizable conditions.

Consider the coexistence of two homogeneous zones "a" and "b" with area γA and $(1 - \gamma)A$, respectively. For simplicity, we assume that all surfactants have the same fixed area per headgroup a_0 and charge either $+e$ or 0. We must compute the equilibrium value γ_* of the fractional area coverage in terms of the ambient salt concentration $\hat{n}$, the dielectric charge density σ_-, the average membrane composition $\sigma_{+,\mathrm{av}}$, and the headgroup area a_0. We will show that the effective charge in zone "b" is negative.

Examining Fig. 2, we see that each zone freely exchanges two independent conserved quantities with the other. We may take these to be the net counterion charge Q_1 below the membrane and the total surfactant charge Q_+ of the membrane itself, with corresponding areal charge densities σ_1 and σ_+, respectively (11). We express all densities in dimensionless form, letting $\sigma_{\max} = 2e/a_0$ and $\bar{\sigma}_1 = \sigma_1/\sigma_{\max}$, and so forth. Thus, $\bar{\sigma}_+$ must obey the important conditions $0 < \bar{\sigma}_+ < 1$, while $\bar{\sigma}_1$ is (in principle) unbounded.

To make the formulae as transparent as possible, we first study the hypothetical case of a very thin membrane. We must compute the free energy density of a homogeneous region at fixed charge density, and then apply the usual phase coexistence rules. To get f, we simply add three terms, letting $f = f_1 + f_0 + f_m$, where:

1) f_1 is the free energy of the half-infinite space inside the vesicle. This space sees a plane of charge density $-\sigma_1$, so in Debye-Hückel theory, its free energy cost is $f_1 = (\sigma_{\max}^2/2\kappa\epsilon)\bar{\sigma}_1^2$.

2) f_0 is the free energy of the gap region. This space sees a plane of charge σ_-, a gap of width ℓ, and another plane of total charge $\sigma_t \equiv \sigma_+ + \sigma_1$. Minimizing the free energy over ℓ gives in Debye-Hückel theory (8) $f_0 =$

$$\frac{\sigma_{max}^2}{2\kappa\epsilon}\left[\bar{\sigma}_-^2 + \bar{\sigma}_1^2 + \bar{\sigma}_t^2 + \bar{W}\right].$$ As discussed

above, the nondimensional adhesion energy $\bar{W}$ equals $-2\bar{\sigma}_-^2$ if $\bar{\sigma}_t > |\bar{\sigma}_-|$, $-2\bar{\sigma}_t^2$ if $0 < \bar{\sigma}_t < |\bar{\sigma}_-|$, or zero if $\bar{\sigma}_t < 0$. The third case corresponds to the possibility of a charge-reversed state with equilibrium spacing $\ell_* = \infty$ (zone "b" of Fig. 2D).

3) f_m is the free energy density of the membrane itself. We retain only the entropy of mixing of charged and neutral surfactants, and neglect any other entropic or enthalpic packing effects in the membrane's free energy. Thus, we have the simple form $f_m = \frac{2}{a_0} k_B T [\bar{\sigma}_+ \log \bar{\sigma}_+ + (1 - \bar{\sigma}_+) \log(1 - \bar{\sigma}_+)]$.

The mixing entropy term f_m opposes phase decomposition, whereas the electrostatic terms $f_1 + f_0$ promote it. The dimensionless ratio $\beta \equiv 2\kappa\epsilon k_B T/e\sigma_{\max}$ describes

the relative importance of these effects. Because typical surfactants have $\sigma_{\max} = e/0.6$ nm², a 1 mM NaCl solution with $\kappa^{-1} \approx 10$ nm gives $\beta \approx 0.006$. We may thus expect to find two-phase coexistence, and indeed, inspection of the free energy density reveals such an instability (Fig. 3). [In the figures, we have plotted the exact Poisson-Boltzmann theory result (7); these results are qualitatively similar to those derived from the simple, linearized Debye-Hückel formulae given above (12).]

Using for illustration the values $\bar{\sigma}_{+,\mathrm{av}} = 0.5$ and $\bar{\sigma}_- = -1.5$ then gives (7) coexistence between an adhesion zone with $\bar{\sigma}_+^{(a)} = 0.95$, covering a fraction $\gamma_* = 36\%$ of the vesicle, and a charge-reversed zone with $\bar{\sigma}_+^{(b)} = 0.25$. The latter zone presents total charge density $\bar{\sigma}_t = -0.12$ to the outside of the vesicle (thus reversed in sign), or about -45% of the value $\sigma_{+,\mathrm{av}}/2$ presented to the outside when the adhering dielectric is far away.

To treat a realistic (finite-thickness) membrane, we must distinguish the two halves of the bilayer. Intuitively, one may expect that for a very thick membrane the energy cost of putting electric field lines in the dielectric interior of the membrane would become prohibitive, so that the system stops at Fig. 2C instead of proceeding to Fig. 2D. We now show that realistic membranes are not so thick, and do exhibit the same charge reversal (to a reduced degree) as the thin case just discussed.

Let the inner monolayer have charge fraction $u\bar{\sigma}_+$ and the outer $(1 - u)\bar{\sigma}_+$. Bilayer membranes have capacitance per area of around $c = 0.01$ pF/µm² (5), so we modify our free energy density f by adding a capacitive term $f_c = \frac{\sigma_{\max}^2}{2\kappa\epsilon}\tau(\bar{\sigma}_1 + u\bar{\sigma}_+)^2$ where the dimensionless ratio $\tau \equiv \kappa\epsilon/c$ measures the importance of membrane thickness. Using for illustration a 1 mM NaCl electrolyte then gives $\tau \approx 7$. We must also replace f_m by the corresponding formula for two layers.

For given $(\bar{\sigma}_+, \bar{\sigma}_t)$, we first minimize $f(\bar{\sigma}_+, \bar{\sigma}_t, u, \ell)$ over ℓ and u, then repeat the phase-coexistence analysis. The free energy surface is then qualitatively similar to Fig. 3, although the extent of coverage in equilibrium γ_* is larger, around 63% (13). The degree of charge-reversal is now smaller, about -1.2% of the value $\sigma_{+,\mathrm{av}}/2$. Even this small effect causes vigorous rejection of additional adhering objects: Increasing the adhesion area beyond its preferred value $A\gamma_*$ by 1 µm² on a vesicle of radius 10 µm comes at a net free energy cost of more than $3000k_BT$. Decreasing the area below $A\gamma_*$ by removing a ball comes at a similar cost. Thus, realistic membranes can partition into an adhesion zone and a charge-reversed, repulsive, zone.

Our result is relatively insensitive to the

values of the charge densities σ_- and $\sigma_{+,\mathrm{av}}$, although we must have $|\sigma_-| > \sigma_{+,\mathrm{av}}/2$ in order to obtain the instability. Increasing the salt concentration beyond $\hat{n} = 20$ mM, however, eliminates charge reversal by increasing τ, a prediction in qualitative agreement with the experiments of (3). If $\hat{n}$ lies between 20 mM and ~150 mM, we still find an instability, this time to partitioning into strong- and weak-adhesion zones (2).

In retrospect, our mechanism is reminiscent of the chemiosmotic principle in bioenergetics (14): In this context it is well known that electrostatic effects can be transmitted over many screening lengths with the help of a semipermeable membrane. Besides entering into an explanation of the experiments in (2, 3), our mechanism predicts that flaccid charged vesicles can adhere to oppositely charged substrates while remaining flaccid. Our analysis also makes testable predictions about the dependence of the equilibrium area fraction γ_* on the system parameters, notably the bilayer composition and salt concentration. Perhaps most strikingly, the charge-reversed zone we describe should prove attractive to same-charge objects—a phenomenon not yet seen.

References and Notes

1. S. A. Safran, *Statistical Thermodynamics of Surfaces, Interfaces, and Membranes* (Addison-Wesley, Reading, MA, 1994).
2. J. Nardi, R. Bruinsma, E. Sackmann, *Phys. Rev. E* **58**, 6340 (1998).
3. L. Ramos, T. C. Lubensky, N. Dan, P. Nelson, D. A. Weitz, unpublished results.
4. Changes in the materials used had little effect on the experimental results in (3). We used colloidal spheres of diameters 0.98, 0.83, and 1.00 μm, with sulfate groups, sulfate and carboxylate groups, and carboxylate and amine groups, respectively. Electrophoretic velocity measurements confirmed that all types of particles were negatively charged in our experimental conditions. All three samples behaved similarly in the experiments. We also varied the bilayer characteristics through the addition of octanol. Although this co-surfactant is known to alter the curvature-elasticity properties of bilayers, we could not see any qualitative effect on our results at alcohol-to-Triton-X weight ratios ranging from 0 to 0.7. In Fig. 1, the weight ratio DDAB (didodecyl dimethyl ammonium bromide):Triton:octanol was 1:0.37:0.13. The buffer solution contained NaCl at concentrations from 1 to 10 mM, as discussed below.
5. R. B. Gennis, *Biomembranes* (Springer-Verlag, New York, 1989).
6. W. M. Gelbart and R. Bruinsma, *Phys. Rev. E* **55**, 831 (1997).
7. Y. Chen and P. Nelson, unpublished results.
8. V. A. Parsegian and D. Gingell, *Biophys. J.* **12**, 1192 (1972).
9. We work in SI units. Thus, $\epsilon_0 = 9 \times 10^{-12}$ F/m, the potential around a point charge q in vacuum is $\psi(r) = q/4\pi\epsilon_0 r$, and so forth.
10. We need not assume the membrane to be impermeable to water; because the bulk salt concentration is assumed the same on both sides, there will be no net osmotic flow.
11. A third exchanged quantity, the net counterion charge density outside the membrane, is then fixed by charge neutrality: $\sigma_0 = -(\sigma_1 + \sigma_+ + \sigma_-)$. Similarly, the density of neutral surfactants in the membrane is not independent, being given by $(2/a_0) - (\sigma_+/e)$. The numbers of individual counterions of each species are not, however, conserved,

because neutral $+/-$ pairs can be exchanged with large reservoirs (the bulk solution inside and outside the vesicle) without macroscopic charge separation.
12. Poisson-Boltzmann theory is a mean-field approximation. It is well known that correlated fluctuations can cause surprising effects if the counterions are multivalent. For example, like-charged parallel plates can have attractive regimes (15, 16), although we are not aware of a similar prediction of repulsion for opposite charges. Correlation effects are generally small if the ions are univalent, as in the experiment of (3). The physical mechanism we present, in contrast, arises already in mean-field theory; it does not rely on any fluctuation effects (nor on finite ion-size effects). Including such effects does not materially change our conclusions (7). Other colloidal forces not included in our analysis (for example solvation forces) are short-ranged; our effect relies on the physics of surfaces when they are separated by more than a nanometer.
13. The extent of coverage is not directly measurable, since the degree to which each colloidal sphere is engulfed by membrane is not observed. In addition,

the actual situation in Fig. 1 may not be in equilibrium. Our point is simply that our theory explains why the vesicle in Fig. 1 has stopped attracting further colloidal particles.
14. R. J. Nossal and H. Lecar, *Molecular and Cell Biophysics* (Addison-Wesley, Redwood City, CA, 1991).
15. L. Guldbrand, B. Jönsson, H. Wennerström, P. Linse, *J. Chem. Phys.* **80**, 2221 (1984).
16. I. Rouzina and V. A. Bloomfield, *J. Phys. Chem.* **100**, 9977 (1996).
17. We thank R. Bruinsma and S. Safran for discussions; J. Crocker, K. Krishana, and E. Weeks for experimental assistance; and J. Nardi for communicating results to us before publication. N.D. was supported in part by NSF grant CTS-9814398; T.C.L., L.R., and D.A.W. were supported in part by NSF Materials Research and Engineering Center Program under award number DMR96-32598 and equipment grants DMR97-04300 and DMR97-24486; P.N. was supported in part by NSF grant DMR98-07156; L.R. was supported in part by a Bourse Lavoisier from the Ministère des Affaires Etrangères de France.

Climate and Satellite Indicators to Forecast Rift Valley Fever Epidemics in Kenya

Kenneth J. Linthicum,[1]* Assaf Anyamba,[2]* Compton J. Tucker,[2] Patrick W. Kelley,[1] Monica F. Myers,[2] Clarence J. Peters[3]

All known Rift Valley fever virus outbreaks in East Africa from 1950 to May 1998, and probably earlier, followed periods of abnormally high rainfall. Analysis of this record and Pacific and Indian Ocean sea surface temperature anomalies, coupled with satellite normalized difference vegetation index data, shows that prediction of Rift Valley fever outbreaks may be made up to 5 months in advance of outbreaks in East Africa. Concurrent near–real-time monitoring with satellite normalized difference vegetation data may identify actual affected areas.

Rift Valley fever (RVF), a viral disease first described in Kenya in 1931 (1), affects domestic animals and humans throughout sub-Saharan Africa and results in widespread livestock losses and frequent human mortality. Its occurrence is known to follow periods of widespread and heavy rainfall associated with the development of a strong intertropical convergence zone, the region in the equatorial tropics where air currents from the north and south converge and produce precipitation (2). Such heavy rainfall floods mosquito breeding habitats in East Africa, known as "dambos," which contain transovarially infected *Aedes* mosquito eggs and subsequently serve as good habitats for other *Culex* species mosquito vectors (3). The most recent RVF

[1]Department of Defense, Global Emerging Infections System, Division of Preventive Medicine, Walter Reed Army Institute of Research, Washington, DC 20307–5100, USA. [2]Earth Sciences Directorate, NASA Goddard Space Flight Center, Greenbelt, MD 20771, USA. [3]Special Pathogens Branch, Centers for Disease Control and Prevention, Atlanta, GA 30333, USA.

*To whom correspondence should be addressed.

epizootic/epidemic was in East Africa in late 1997 and early 1998.

Vegetation responds to increased rainfall and can be easily measured by satellite. Normalized difference vegetation index (NDVI) data from the advanced very high resolution radiometer (AVHRR) on National Oceanic and Atmospheric Administration (NOAA) satellites have been used to detect conditions suitable for the earliest stages in an RVF epizootic (4). Refinement in determining the spatial distribution of RVF viral activity, through identification of ideal mosquito habitat, has been possible with higher resolution Landsat, Systeme pour l'Observation de la Terre (SPOT), and airborne synthetic aperture radar data (5); however, predictive indicators are needed to forecast RVF outbreaks. Here we show that several climate indices can be used to predict outbreaks up to 5 months in advance.

The El Niño–Southern Oscillation (ENSO) phenomenon is a principal cause of global interannual climate variability (6, 7). Warm ENSO events are known to increase precipi-